論文 / 著書情報
Article / Book Information

Title	Mechanical consequence observation and microscopic visualization of internal erosion using developed plane strain erosion apparatus
Authors	Mao Ouyang, Akihiro Takahashi
Citation	Geotechnical Testing Journal, Vol. 45, No. 2, pp. 411-431
Pub. date	2022, 3
Copyright	This is a preprint of an article published in Geotechnical Testing Journal, (c) 2022, ASTM International, West Conshohocken, PA, http://dx.doi.org/10.1520/GTJ20200298, www.astm.org.

Mechanical consequence observation and microscopic visualization of internal erosion using developed plane strain erosion apparatus

Mao Ouyang[1], and Akihiro Takahashi[2]

ABSTRACT

Internal erosion has been frequently reported and has caused failures and instabilities of geotechnical structures. A plane strain erosion apparatus is developed in this study to allow the subsequent conduction of drained compression test after seepage test, and the microscopic observation of particle movement through a transparent window. A drained compression test preceded by a seepage test is performed on specimens containing the same initial fines contents to investigate the mechanical consequence impacts of seepage-induced internal erosion. Experimental results reveal that compared with uneroded soils, internally eroded soils show a larger secant stiffness at a small strain level (~1 %). At medium strain level (~15 %), the soils with erosion show smaller deviator stress comparing with soils without erosion. The analysis of images recorded by the microscope proves that the fines contacted with coarse particles possibly transferring the load are distinct between the soils with and without internal erosion at both small and medium strain levels during the drained compression test, which indicates that the soil fabric could affect the mechanical behaviors of soils subjected to internal erosion. Our designed equipment and microscopic observation could throw some light on the research of internal erosion from the view of particle scale.

Keywords

Plane strain erosion apparatus; internal erosion; microscopy; stiffness; stress analysis; soil fabric.

Geotechnical Testing Journal 45 (2), 411-431, 2022
Official URL:
https://doi.org/10.1520/GTJ20200298

[1] Department of Environment Systems, Graduate School of Frontier Sciences, The University of Tokyo, Chiba, Japan (Formerly, Tokyo Institute of Technology, Tokyo, Japan), ORCID: 0000-0002-5967-462X
[2] Department of Civil and Environmental Engineering, Tokyo Institute of Technology, Tokyo, Japan; ORCID: 0000-0003-1206-5066

Introduction

Evaluation of the safety of some geotechnical structures, such as embankments and dams, are often based on the assumption that the components of solid fracture are static. The changing climate has resulted in severe inundation and infiltration into the soils (Hirabayashi et al., 2013; Ouyang et al., 2020, 2021a,b), which has caused internal erosion and subsequent instabilities and failures (Foster et al., 2000). Internal erosion is defined here as the transport of detached finer particles through the soil mixtures under seepage flow (Bonelli, 2012), which would cause soils mass loss, volume change and hydraulic conductivity alteration from the viewpoint of macro-scale (Fannin and Slangen, 2014; Slangen and Fannin, 2017). Microscopically, internal erosion could lead to the transportation and local accumulation of fines within soil mixtures, mobilization of particles positions and change of the void volume (Fannin and Slangen, 2014; Slangen and Fannin, 2017; Ouyang, 2016). Elementary test apparatus has been developed to investigate the physical and mechanical features of internal erosion. Systematic visual observation has been employed to interpret the different mechanical consequences of soils with and without internal erosion.

Besides the studies performed to examine the criteria for soils likely to develop internal erosion (Kenney and Lau, 1985; Foster and Fell, 2001; Zhong et al., 2018), many experimental devices were developed and laboratory tests were conducted to understand the physical and mechanical behaviors of soils suffering internal erosion (Skempton and Brogan, 1994; Tomlinson and Vaid, 2000; Horikoshi and Takahashi, 2015). Xiao and Shwiyhat (2012) investigated the undrained behavior of internal eroded soils by triaxial apparatus with a revised pedestal to allow the dislodgement of fine fractions. Based on the hydraulic gradient changes during the internal erosion, Chang and Zhang (2011) divided the internal erosion into four

stages: stable, initiation, development and failure, by providing the pressurized seepage flow in a revised triaxial device. Ke and Takahashi (2014b) further revised the triaxial apparatus by supplying the back pressure into the sedimentation tank to ensure the high saturation degree of tested specimens experienced internal erosion. Except for the modified triaxial cells, Richards and Reddy (2010) developed a true triaxial piping test apparatus to evaluate the erosion potential of small to middle embankments. The true triaxial test results demonstrated that an increase in maximum principal stress and seepage angle and a decrease in the void ratio would cause an increase in the seepage velocity initiating the internal erosion (Richards and Reddy, 2012).

With the developed experimental apparatus, the mechanical consequences of soils subjected to internal erosion were reported. The triaxial drained compression tests on soils with and without erosion were conducted by Ke and Takahashi (2014a), results of which revealed that with the progress of internal erosion, the hydraulic gradient would decrease and hydraulic conductivity would increase. Further examination performed by Ke and Takahashi (2016) suggested that internal erosion could decrease the peak strength of cohesionless soils. Chen et al. (2016) performed drained compression tests on soils using the dissolved salt to represent the eroded fines. They reported that the peak friction angle and critical friction angle would decrease after fines losing, and the stress-strain response changed from dilative to contractive. Ouyang and Takahashi (2016a,b) compared the undrained compression behaviors of soils with and without erosion containing the same initial fines contents in a revised triaxial cell. They showed that the secant stiffness of soils with erosion was larger than that of soils without erosion at the small strain level. The undrained peak strength and residual strength were also changed by internal erosion. Similar results on specimens with a wide range of initial fines content were reported by Prasomsri and Takahashi (2020).

The experimental results have shown that the internal erosion would affect the physical and mechanical behaviors of soils, thus, many researchers tried to examine the differences from the systematic visual observations (Hunter and Bowman, 2018; Dumberry et al., 2018; Xie et al., 2018). The image subtraction approach was employed by Rosenbrand and Dijkstra (2012) to quantify the fines mobilization and transportation in a saturated plane strain porous medium. The results indicated that fines movement during internal erosion changes over time under constant flow boundary conditions. The transportation and removal of fines from the soils seemed to be localized due to the positive feedback effects. Ouyang and Takahashi (2015) optically quantified the feature of internal erosion in the plane strain physical models. They noted that fines were prone to be transported within an instant period of increasing hydraulic gradient, with few of them moving during the constant flow. The volume of specimens was reduced due to internal erosion, which resulted in an alteration of preferred coarse particle orientations in the observation field.

Numerical studies were also employed to interpret the effects of internal erosion on the soils mechanical behaviours. In terms of simulations within a discrete framework, the influence of confining pressure and fines content on the internal erosion of gap graded soils was investigated by a coupled CFD-DEM method (Liu et al., 2020). Zou et al. (2020) used a similar approach and noted that internal erosion caused a sharp reduction of fines in the bottom layer, while a slight decrease of fines in the upper layers. Yang et al. (2019b) proposed a four-constituent continuum model: solid skeleton, the erodible fines, the fluidized particles, and the pure fluid, to examine the effects of internal erosion on the safety of earthen structures. The erosion process was modeled based on the discharge of the fluidized particles (Yang et al., 2019c). To consider the soil's spatial variability, Yang et al. (2019a) introduced the random field

theory to investigate the internal erosion with randomly distributed initial porosity and fines contents. They reported that the assumption of soil homogeneity was insufficient to predict the decrease of the hydraulic conductivity during the internal erosion. A similar approach was employed by Yang et al. (2020), they compared the numerical simulation results with the experiment results, and mentioned that the specimens heterogeneity would affect the critical hydraulic gradient and delay of the final equilibrium state and more laboratory tests were beneficial for the further development of internal erosion modeling.

Although apparatus have been developed and techniques have been utilized to examine the characteristics of internal erosion, discovering the mechanism from the micro-scale/particle scale to the macro scale is still challenging. In this contribution, we develop a plane strain erosion apparatus equipped with a visible window to allow direct microscopic visualization and stress measurements in three directions. The drained compression tests are conducted in soils containing the same initial fines contents with and without seepage tests to show the effects of seepage-induced internal erosion on the physical and mechanical behaviors. An analysis based on the images recorded by the microscope is performed to explain the different mechanical behaviors from the perspective of particles contact.

Plane Strain Erosion Apparatus

APPARATUS DEVELOPMENT

To unravel the mechanical behavior of soils subjected to seepage-induced internal erosion, one of the main difficulties lies in the direct observation of particles movement and its relative positions during the seepage and compression tests. The other one is the application of surrounding stresses on the soils during the seepage tests since internal erosion often occurs in

93 geotechnical structures subjected to earth pressures. Moreover, a non-destructive approach is
94 necessary for the quantification of the particles interface movement and the connection between
95 the micro-scale behaviors and macro-scale consequences. Upon these difficulties, we develop a
96 plane strain erosion apparatus, the schematic diagram of which is presented in Fig. 1. The
97 photography of the main components of the plane strain erosion apparatus is shown in Fig. 2.
98 The plane strain erosion apparatus is designed based on the revised triaxial erosion apparatus (Ke
99 and Takahashi, 2014b) to microscopically observe the characteristics of internal erosion under
100 plane strain conditions. Both seepage and drained compression tests can be performed in the
101 developed equipment.

102 It mainly consists of a plane strain cell, a seepage control unit and a pressure control unit.
103 A transparent acrylic window is assembled in the front of the plane strain cell to enable the
104 tracking of particles transportation. Transparent membranes are employed in this research to
105 enclose the soils.

106 The seepage control unit consists of a water reservoir, a flow pump and a sedimentation
107 tank. The water reservoir is used to provide the water for the seepage test. The water is prepared
108 at least 24 hours before conducting the experiments and is kept at room temperature. The
109 seepage test performed in the developed plain strain apparatus is controlled by flow rate, because
110 the application of flow rate in seepage-induced internal erosion could provide consistent results
111 (Richards and Reddy, 2010). To maintain the constant flow rate during the seepage test, all the
112 flow channels are designed to be the same size. The top cap is fabricated with a conical tough,
113 and a perforated plate is mounted to be directly attached to the top surface of the specimen (Fig.
114 3(a)). The pedestal is symmetrically made with an inverted conical tough and a perforated plate
115 (Fig. 3(b)), to maintain the constant flow rate and minimize the water head loss. The opening

size of the perforated plate is 1 mm in this apparatus, which could fully hold the coarse particles and permit the dislodgement of fines (Ouyang and Takahashi, 2016a). The apertures are uniformly distributed in both the top cap and pedestal, plus that the specimen is enclosed by the flexible membrane, which could possible avoid some preferential flow that typically observed in the test using a fixed-wall permeameter along the transparent window. The eroded fine particles and the effluent water would be collected by the sedimentation tank (Fig. 1), which could be pressurized to simulate any reasonable downstream pressure or be open to the atmosphere. In this research, the downstream pressure is maintained at atmospheric pressure. The cumulative eroded soil mass is gained by continuously weighing the light tray, which is fully submerged in the sedimentation tank. During the trial test, we found that the fluid caused some impact effects on the light tray, which disturbed the measurement of the eroded mass. To minimize the influence, we put a funnel with a 15 mm diameter opening at the end of the inlet pipe. The position of the funnel outlet is aligned with the tray center. The miniature load cell installed in the sedimentation tank, which is waterproof and has a high sensitivity, could record the cumulative eroded soil mass within a continuous period. The theoretical capacity of the miniature load cell is 500 g; the precision of the miniature load cell is 0.01 g.

eroded soil mass, and the normal stress in the di $_{yy}$). After the seepage test, the soil volume is measured to obtain the volumetric strain caused by seepage-induced internal erosion. For the drained compression tests, the axial stress, and soil deformation in both vertical and ho $_{xx}$) are recorded.

TESTED MATERIALS

The tested specimens are 70 mm wide, 70 mm deep and 100 mm high. The materials are a mixture of blue-colored silica no. 8 and natural silica no. 3, which are mainly composed of quartz, and categorized as sub-round to sub-angular materials. Silica no. 3 has a large grain size, forming the skeleton of the soil specimens, which is regarded as coarse particles. Silica no. 8 is artificially coated with blue pigment, and then stabilized by baking. It is regarded as fines, which could be eroded by seepage flow in the gap-graded mixtures (Zuo and Baudet, 2015). All the soil mixtures are prepared with 25 % initial fines content by moist tamping method (Ladd, 1978) with the non-linear undercompaction criteria (Jiang et al., 2003), which has been proved to be able to generate uniform soil specimens in laboratory experiments (Ke and Takahashi, 2014b). The specimens are prepared with 42 % relative densities. The permeabilities of the specimens with 25 % initial fines content are 2.4×10^{-3} cm^2 (Freeze and Cherry, 1979; van Baaren, 1979). The properties of individual sand and mixed sands are shown in Table 1. The particle size distribution curves of soils based on the sieve test (ASTM D6913 / D6913M-17, 2017) are presented in Fig. 4, together with the microscopic image of particles. The image demonstrated that the contours of both fines and coarse particles can be observed by the microscope under the transparent membrane and acrylic window installed in the front of the plane strain erosion apparatus.

Base on the numerical analysis performed by Shire et al. (2016), and the experimental

work conducted by Lade et al. (1998) and Choo et al. (2018), the size ratio of D50/d40 can be regarded as a criterion to define the transition of soil fabric, where D50 is the coarse particle size with 50 % finer and d40 is the size of the fines with 40 % finer. When the size ratio of D50/d40 was larger than 6, the soil mixtures could be regarded as gap-graded soils (Skempton and Brogan, 1994; Shire et al., 2016), where the contacts between fines and coarse particles depend on the fines content. In this study, the size ratio of the specimen equals 18, which presents a metastable transit state. The fines content was chosen as 25 %, which is smaller than the fines content where fines separate the coarse particles (35 %) (Shire et al., 2016). In this case, some fines carry reduced effective stress which might be transported by the seepage flow under appropriate conditions, and the mechanical consequences of the whole soils with and without internal erosion can be distinguished by the developed apparatus.

EXPERIMENTAL PROCEDURE

The experimental procedure of the plane strain erosion test includes saturation, consolidation, seepage, and drained compression tests. The stress path is shown in Fig. 5. The first number in the bracket means the horizontal normal stress perpendicular to the plane strain xx yy); the last o zz).

Saturation

The vacuum saturation procedure is employed in this study. Two separated reservoirs are connected to the top and bottom of the specimens. After soils preparation, vacuum is applied gradually until it reaches -20 kPa (equals to 20 kPa applied to the specimen in Fig. 5). In the test, a noticeable change of the particles arrangement by the vacuum pressure application was not observed, thus, we regard that -20 kPa vacuum pressure application would hardly cause the

185 modification of particles arrangement and void repartition from the initial state. Deaired water is
186 then infiltrated into the soils from the bottom to the top. The velocity of flow is sufficiently slow
187 (2.8×10^{-5} m/s) to avoid the segregation of fines from the coarse particles. After around 10 times
188 of the pore volume is flowed through deaired water, the saturation process is finished.

189 **Consolidation**

190 The consolidation is performed with a feedback control system. $_{xx}$ is gradually increased
191 up to the target value (50 kPa in this study) at a fairly low increment (1 kPa/min) to avoid the
192 $_{zz}$), controlled by a motor, is programmed to be
193 $_{xx}$ and is smoothly increased to 50 kPa (Fig. 5).

194 **Seepage Test**

195 Upon the finish of consolidation, the seepage test is conducted on specimens aiming to
196 investigate the features of internal erosion. It is controlled by multistage flow rates based on the
197 advantage of providing continuous flow within a relatively long period. The first to the third
198 stage of the seepage test is terminated based on the criteria that within 600 s, 1) the effluence
199 become clear and clean; 2) no further eroded fines could be measured; 3) no further specimen
200 deformation could be measured; 4) no movement of particles could be observed by the
201 microscope. The final stage (stage 4) is applied with the maximum capacity of the pump with
202 flow rate equals to 6.5×10^{-6} m^3/s, until all the water in the reservoir (5.3×10^{-2} m^3) are used in
203 the seepage test, to allow more fines eroded away. The period of each stage is determined by the
204 above criteria for the first experiment. In repeated case, the same period is employed, but some
205 changes in the eroded soil mass are observed even near the end of stage 4. Figure 6 shows the
206
207 shown in Fig. 5). The cumulative eroded soil mass is recorded by the miniature load cell installed

in the sedimentation tank (Fig. 1). The microscopic images are recorded during each stage of seepage tests at various designed height by a microscope VCR-800 (Product by Hirox) (Ouyang and Takahashi, 2015).

Drained Compression Test

The drained compression test is displacement controlled with an axial strain rate increment of 0.1 %/min (in the direction of $_{zz}$) according to the standard criteria of the drained triaxial test (ASTM D7181-11, 2011). The stress-strain relationship and the axial strain against deviator stress are obtained from the drained compression test. During the compression tests, a series of microscopic images are recorded to investigate the movements and relative positions of both fines and coarse particles.

TEST CONDITIONS

The test conditions presented in this article are listed in Table 2. For the case name, PS means the plane strain test, CON means the consolidation test, WE and WOE represent with and without application of seepage test, respectively, N1 and N2 mean the number of tests. To examine the effectiveness of the preparation method, case PS_CON is ended after the consolidation. Case PS_WOE is performed to investigate the drained compression behaviors of soils without erosion. Seepage and subsequent drained compression test are conducted twice to validate the repeatability, corresponding to cases PS_WE_N1 and PS_WE_N2.

Experimental Results

OPTICAL RESULTS

The photos of the whole specimens before, during, and after seepage test of case PS_WE_N2 are presented in Figs. 7(a), (b), and (c), respectively. The dislodgement of fines

could be clearly observed through the transparent membrane and acrylic window. Figure 7(d) shows the apparatus after the drained compression test, the specimen is compressed to around 15 % axial strain. Two monotone microscopic images recorded at the same position before and after the seepage test are presented in Figs. 7(e) and (f), a comparison of which indicates that the fines are transported outside the scope of the microscope.

SEEPAGE TEST RESULTS

After the consolidation, the void ratios of soils in case PS_CON are measured in five equivalent layers. The soils in each layer are oven-dried at 100^{o}C for 24 hours. The targeting void ratio is 0.60, and the measured void ratios from the bottom to the top are 0.61, 0.53, 0.61, 0.63, and 0.59. The good agreement between the measured void ratios and target void rations suggests that specimens prepared by the moist tamping method with non-linear undercompaction theory could achieve reasonable homogeneity (Ouyang, 2016). A summary of seepage test results is shown in Table 3. After the seepage test, the vertical displacement of the top cap, and the average horizontal displacement of the water bladders which confined the soil specimen, are measured. The vertical displacement represents the vertical deformation of the specimen. The average horizontal displacement of the water bladders represents the horizontal displacement of the specimen in the $_{xx}$ direction. The specimens show contractive behaviors in both vertical and $_{xx}$) directions. The vertical and horizontal displacements are 0.8 mm and 1.0 mm for case PS_WE_N1, and 0.9 mm and 0.9 mm for case PS_WE_N2. The void ratio increases, corresponding to a decrease of relative density, suggesting the specimens become loose after seepage tests.

The grain size distributions along the specimen after erosion are measured and presented in Fig. 8. To examine the spatial distribution of fines induced by internal erosion, the specimen is

divided into several parts. The illustration of the divided parts in the case PS_WE_N2 is shown in Fig. 8(a). The top, middle and bottom layers are divided equally to investigate the fines distribution along the length of the specimen. In each layer, two parts are divided, named T1, T2 in the top layer, M1, M2 in the middle layer and B1, B2 in the bottom layer, in order to examine the influence of the boundary conditions. T2, M2 and B2 are the portions near the water bladders, which means they are subjected to flexible boundary conditions.

Figure 8(b) shows the particle size distribution curves in the top, middle and bottom layers. It can be observed that the fines distributions in these three layers are not the same, which suggests that the internal erosion would cause an inhomogeneous specimen under the plane strain condition. For the bottom layer, the particle size distribution curves of B1 and B2 parts are plotted in Fig. 8(c). It is noted that although in the same layer, the fines spatial distributions are affected by the boundary conditions. B2 part shows larger fines loss than B1 part, which means that the locations near the flexible boundary indicate larger fines loss than the other locations.

The evolution of $_{yy}$ at the beginning 4,000 s for case PS_WE_N1 is shown in Fig. 9. It can be found that with the application of seepage flow, $_{yy}$ decreases. We can also note that the variations in $_{yy}$ correspond to the sudden increases of the cumulative eroded soil mass. This might because that the seepage-induced fines transportation inside the soil matrix is not a uniform process due to the different sizes of particles and constrictions. Some fines might accumulate in the constrictions formed by coarse particles. When more and more fines are transported to these constrictions, the fluid impacts would increase. Some fines would be dislodged out to the sedimentation tank and measured by the miniature load cell when the force is larger than the capacity of the constrictions, which corresponds to the sudden increase of cumulative eroded soil

$_{yy}$) presents a pulse shape, but it disappears after the sudden increase of eroded mass.

The evolution of the cumulative eroded soil mass during the whole seepage tests for cases PS_WE_N1 and PS_WE_N2 are shown in Fig. 10(a). Two cases showed similar trends in the progress of seepage tests and soil masses at the end of tests, suggesting the seepage tests performed by the developed planes train erosion apparatus could yield consistent results. Figure $_{yy}$ during the seepage tests. It is found that with the dislodgement of fines $_{yy}$ decreases correspondingly in this study. The permeability increases with the process of fines dislodgement, as demonstrated in Fig. 10(c).

The measurement during the experiments would include uncertainties, to examine the effects of the uncertainties on the results, we conduct the experiments with 25 % initial fines content twice. The measured total seepage-induced eroded soil mass and the decreasing trend of $_{yy}$ of the two cases are similar, which demonstrates that the repeatability of the developed plain strain apparatus is acceptable for this study.

DRAINED COMPRESSION TEST RESULTS

For the case PS_WOE, the drained compression test is performed after the consolidation. For the cases PS_WE_N1 and PS_WE_N2, the drained compression tests are performed subsequently after the seepage tests. The relation of axial strain and volumetric strain during drained compression test is shown in Fig. 11(a). It is noted that both soils with and without erosion showed contractive volume deformation. During the seepage test, only the fines are eroded away through the perforated plate, the amount of coarse particles for the eroded and non-eroded are identical. At the medium strain level, fines might be pushed into the voids between coarse particles and the contacts between coarse particles dominant the volume of the specimens,

300 which probably lead to similar volumetric strains of eroded specimen compared with the non-
301 eroded specimen (Zlatovic and Ishihara, 1997). The experiments performed by Ke and Takahashi
302 (2016) also noted that the soils with and without seepage-induced internal erosion present quite
303 similar volume changes during the drained compression tests.

304 Figure 11(b) presents the relationship between axial strain and deviator stress during the
305 whole compression tests. The enlarged profile of axial strain between 0 and 2 % (Fig. 11(c))
306 notes that when the axial strain was less than around 1 %, the deviator stress of soil with erosion
307 is larger than that of soil without erosion at the same strain. This suggests that the seepage-
308 induced internal erosion would affect the soil stiffness at a small strain level (Clayton, 2011).
309 Secant stiffness is defined as the gradient of stress-strain curves, which reflects the relationship
310 between the change of deviator stress and the change of axial strain. The normalized secant
311 xx,
312 50kPa in this study). At the small strain level, the soil with erosion shows larger normalized
313 secant stiffness than the soil without erosion, which suggested that internal erosion-induced soil
314 fabric might cause the increase of secant stiffness at small strain level during drained
315 compression (Ke and Takahashi, 2016). Taken the 0.1 % axial strain, for instance, the uneroded
316 soil shows normalized secant stiffness of 50, whereas, the eroded soils show that of 90
317 (PS_WE_N1) and 150 (PS_WE_N2), respectively. Due to the inherent limitation of the test
318 xx will wear the connection between the rubber water
319 bladders and the steel plates, therefore, two post-erosion drained compression tests are ended at
320 around 15 % axial strain. The peak strength here is then defined as the maximum value of the
321 deviator stress. Table 4 shows the summary of drained compression test results of soils with and
322 without erosion. The results reveal that the soils with erosion show smaller peak strength

compared with the soils without erosion in this study.

Discussions

The experimental results reveal that the mechanical behavior of soils with internal erosion is different from that of soils without erosion. The difference of stress responses changes with the levels of axial strain, which indicates that the explanation of the effects of internal erosion is much more complex than what we have perceived. Based on the assumption that the mechanical behaviors of sand mixtures are affected by void ratio and fabric (Zlatovic and Ishihara, 1997; Yang and Liu, 2016), the test procedures are reviewed and the corresponding microstructures of soils with and without erosion at key states are presented in Fig. 12. To compare the fines spatial distributions of eroded and uneroded soils, four key states are selected. For soils with erosion, the key states are WE_A, the state before seepage test; WE_B, state after seepage and before compression test; WE_C, state at small strain level during drained compression test; and WE_D, state at medium strain level (Fig. 12(a)). Correspondingly, the key states of soils without erosion are named WOE_A, WOE_B, WOE_C, and WOE_D (WOE_A and WOE_B are the same since seepage is not applied for the soils without erosion).

It was recognized that soil behaviors could be influenced by the preparation method (Takahashi, 2016). The microstructures in WOE_A and WE_A are derived from an original microscopic image taken in the center of the specimen, where coarse particles are represented as grey ovals, and fines are represented as black circles (Fig. 12(b)). The size of coarse particle in the schematic diagram is the same as that in the original image, whereas, the size of fines is exaggerated for a clear and reasonable demonstration of the transportation and contact. The specimens prepared by the moist tamping method are assumed to be in a metastable state, as

346 demonstrated by Sladen et al. (1985). This structure suggests that the fines are not simply to
347 occupy the voids formed by coarse particles but lay around the contacts between coarse particles.
348 For soils without erosion, during the drained compression test, the fines could be easily pushed
349 away by the applied load due to the metastable state at the small strain level, as demonstrated in
350 WOE_C (Fig. 12(c)). At medium strain level (WOE_D in Fig. 12(c)), the volume of specimens
351 decreases, leading to a reduction of the void ratio. The reduction of void ratio would increase the
352 contacts between coarse particles, indicated as more black and white solid lines between particles
353 compared with WOE_C; and would also probably result in a preferential orientation of contacts
354 in the compression direction. These are responsible for the larger deviator stress at the medium
355 strain level than that at the small strain level.

356 For soils with erosion, some fines are eroded during the seepage test, shown as dashed
357 empty circles in WE_B (Fig. 12(d)), resulting in an increase in the void ratio. The fines are
358 moved internally to the contacts between coarse particles as well, which creates a unique soil
359 structure. At the small strain level, these fines might transfer the load as shown in WE_C (Fig.
360 12(d)). At medium strain level, similar to that of soils without erosion, the decrease of volume
361 and induced reduction of void ratio could lead to more contacts among particles (WE D in Fig.
362 12(d)) and preferential contacts in the compression direction, which results in large deviator
363 stress.

364 The influence of internal erosion on soils microstructures is examined through the
365 comparison between WOE_C and WE_C; WOE_D and WE_D (Fig. 12). At the small strain
366 level, the contacts between coarse particles are the same, whereas, the contacts between fines and
367 coarse particles of soils with erosion are larger than those of soils without erosion (WOE_C and
368 WE_C). It suggests that more fines might be accumulated around the contacts between coarse

369 particles, which could effectively transfer the load and then result in larger normalized secant
370 stiffness for eroded soils comparing to that for uneroded soils. At the medium strain level, the
371 contacts between coarse particles are also the same, but the contacts between fines and coarse
372 particles of soils with erosion are smaller than those of soils without erosion (WOE_D and
373 WE_D). It indicates that the fines in the contacts between coarse particles are smaller for soils
374 with erosion than that for soils without erosion, which causes smaller peak strength for soils with
375 erosion than that for soils without erosion.

376 The schematic discussions reveal that soil fabric, specifically the fines contacted with
377 coarse particles and transferring the loads, is crucial in examining the influence of internal
378 erosion on mechanical behaviors. A series of microscopic images of soils with and without
379 internal erosion are recorded at different strain level sand is utilized to try to explain the different
380 mechanical consequences caused by internal erosion. According to the simplifying assumption in
381 the planar domain, the constriction size is defined as the largest sphere that will pass through a
382 particular void formed by coarse particles (Silveira, 1965; Kenney and Lau, 1985). For the gap-
383 graded soils, some fines could pass through within the constriction size, and the remaining fines
384 might accumulate in the contacts between coarse particles, which are assumed to be able to
385 transfer the loads. The area surrounded by coarse particles where fines possibly transfer the load
386 is then calculated as the area of void confined by coarse particles subtracting the area of
387 constriction size, which is termed as in this study. The demonstration of in terms of the
388 densest and loosest state is shown in Fig. 13. The calculation of the coarse particle void and the
389 constriction size is based on the assumption that the particles are sphere (Silveira, 1965; Kenney
390 and Lau, 1985). The constriction size in the densest state is given by the largest circle which can
391 be inscribed between three mutually touching particles (Fig. 13(a)). The constriction size in the

loosest state was given by the largest circle which can be inscribed between four touching particles (Fig. 13(b)). The diameters of the coarse particle (silica no. 3) can be obtained from the particle size distributions. Based on the diameters and the geometry, the void space and the diameter of the inscribed circle are calculated.

Two factors would affect : particle size and relative density, as indicated in Fig. 14. The soils with larger particle size and relative density would have larger contact areas. The effect of particle size on the contact area is considered in the definition of constriction size. The influence of relative density is accounted through a similar approach of constriction size (Indraratna et al., 2007), which assumes that when the relative density equals zero, the distribution of is the same as that in the loosest state. Thus, at a certain relative density is expressed as:

$$= + \times \times ( ) \quad (1)$$

where is the chosen percentage of , is the relative density, is the area surrounded by coarse particles where fines possibly transfer the load for a given value of the per cent smaller than , and is in the densest and loosest state, respectively, for the same . According to Table 3, the eroded soils showed relative densities equal to 30 %, thus, the distributions of at equals 30 %, densest, and loosest states are shown in Fig. 15. It can be noted that the soils show the largest at the densest state, whereas, smallest at the loosest state under otherwise the same conditions. The controlling is chosen as 0.085 mm^2 for 20 % smaller in the distribution curves (Indraratna et al., 2018), which is employed to compare the fines per cent in at small and medium strain levels by the image analysis techniques.

The images of soils with and without erosion are recorded by the microscope at the initiation, small and medium strain levels during the drained compression tests. Using one image could be singular compared to the whole specimen, therefore, to prove our hypothesis (Fig. 12),

415 we employ more than 100 images in each case to obtain reasonable data. The fines per cent in
416 is obtained through image segmentation and image subtraction algorithm (Ouyang and
417 Takahashi, 2015; Ouyang, 2016). The fines contents of eroded specimens and the intact
418 specimens are different at the beginning of the compression test, therefore, the soils images at
419 both small and medium strain levels are subtracted by those at the beginning of the compression
420 test in order to reduce the biases of image processes and to obtain reliable results, as shown in
421 Fig. 16. With the progress of compression, fines are pushed away from their initial location,
422 results in a reduction of fines percent in at both small and medium strain levels. Observation at
423 a small strain level reveals that the percentage of fines in of soils with erosion is larger than
424 that of soils without erosion. It suggests that more fines accumulated in the contacts between
425 coarse particles possibly transfer the load, which results in larger normalized secant stiffness for
426 the eroded soils than that for uneroded soils. At the medium strain level, the percentage of fines
427 in of soils with erosion is smaller than that of soils without erosion. This might because the
428 fines are transported into the voids created by internal erosion at the medium strain level, leading
429 to a smaller percentage of fines, and further a smaller peak strength for soils with erosion than
430 that for soils without erosion.

431 **LIMITATION**

432 Whether the fines transferred load or not is difficult to be identified only through the
433 relative positions between fines and coarse particles, which is an inherent limitation in discussing
434 the soils mechanical behaviors through the image processing technique. Further development of
435 advanced techniques is necessary to demonstrate the force chains in the granular materials. The
436 area surrounded by coarse particles where fines possibly transfer the load is calculated through
437 the images recorded parallel to the direction of compression load, whereas, fines dislodgement

438 and transportation also occur in the direction of seepage flow (Hunter and Bowman, 2018). Due
439 to the limitation of the developed apparatus, it is difficult to record the images in the horizontal
440 sections, which could be further improved with respect to the laboratory experimental
441 equipment. here is defined in 2D planar, whereas, the soil particles are 3D spheres, which will
442 lead to different distribution curves of . For instance, if the radius of a particle is 1, the confined
443 planar area by three particles in the densest state is 0.16, the loosest state is 0.86; however, in 3D
444 configuration, the confined volume is 0.68 in the densest state, 1.91 in the loosest state. It
445 suggests that specific cautions are needed in the application of . It is admitted that the boundary
446 would affect the fines movement in the seepage test. Although the transparent membrane is
447 applied to provide a flexible boundary condition, fines could be more easily washed out nearby
448 the boundaries than inside the sample (Nguyen et al., 2019). According to the measurement of
449 the particle size distributions along the specimen, we find that the specimen would become non-
450 homogeneous after seepage-induced internal erosion. The proposed schematic diagram could not
451 represent the positions and transportation of both fines and coarse particles everywhere, hence,
452 further research is necessary to examine the soil heterogeneity caused by internal erosion.
453

454 ## Conclusion

455 A plane strain erosion apparatus capable of directly investigating not only the mechanical
456 behaviors of soils subjected to internal erosion but also the characteristics of internal erosion
457 from the particle scale is developed. Repeated cases show similar results in the evolution of
458 cumulative eroded soil mass and normal stress in the direction of plane strain, suggesting the
459 developed apparatus could yield consistent results. During both the seepage and drained
460 compression tests, soil specimens show contractive behaviors. The normal stress in the direction

461 of plane strain is found to decrease correspondingly to the dislodgement of fines. The soils with
462 erosion indicate a different stress-strain relationship from the soils without erosion. The
463 discussions on soil microstructures reveal that the soil fabric, specifically the fines accumulated
464 in the area surrounded by coarse particles possibly transferring the load ( ), plays a crucial role
465 in examining the mechanical consequence impacts of internal erosion. At the small strain level
466 (~1 %), the soils with erosion show more fines percent in , which suggests more fines possibly
467 involves in load transfer and then results in a larger secant stiffness, compared with the soils
468 without erosion. At the medium strain level (~15 %), the percentage of fines in is smaller for
469 soils with erosion than that for soils without erosion. This might due to fines transportation into
470 the voids created by internal erosion, leading to a small peak strength for soils with erosion.
471

472 ## Acknowledgements

473 Support for the first author is provided by a Monbukagakusho (Ministry of Education, Culture,
474 Sports, Science and Technology, Japan) scholarship for graduate students. This work was
475 supported by JSPS KAKENHI grant number 25420498.
476

Reference

ASTM D6913 / D6913M-17 (2017). Standard test methods for particle-size distribution (gradation) of soils using sieve analysis. Technical report, ASTM International, West Conshohocken, PA.

ASTM D7181-11 (2011). Method for consolidated drained triaxial compression test for soils. Technical report, ASTM International, West Conshohocken, PA.

Bonelli, S. (Ed.) (2012). Erosion of Geomaterials. John Wiley & Sons.

Chang, D. and L. Zhang (2011). A stress-controlled erosion apparatus for studying internal erosion in soils. Geotechnical Testing Journal 34(6), 1–11.

Chen, C., L. Zhang, and D. Chang (2016). Stress-strain behavior of granular soils subjected to internal erosion. Journal of Geotechnical and Geoenvironmental Engineering 142(12), 06016014.

Choo, H., W. Lee, C. Lee, and S. E. Burns (2018). Estimating porosity and particle size for hydraulic conductivity of binary mixed soils containing two different-sized silica particles. Journal of Geotechnical and Geoenvironmental Engineering 144(1), 04017104.

Clayton, C. (2011). Stiffness at small strain: research and practice. Géotechnique 61(1), 5–37.

Dumberry, K., F. Duhaime, and Y. Ethier (2018). Erosion monitoring during core overtopping using a laboratory model with digital image correlation and x-ray microcomputed tomography. Canada Geotechnical Journal 55(2), 234–245.

Fannin, R. J. and P. Slangen (2014). On the distinct phenomena of suffusion and suffosion. Géotechnique Letters 4(4), 289–294.

Foster, M. and R. Fell (2001). Assessing embankment dam filters that do not satisfy design criteria. Journal of Geotechnical and Geoenvironmental Engineering 127(5), 398–407.

Foster, M., R. Fell, and M. Spannagle (2000). The statistics of embankment dam failures and accidents. Canada Geotechnical Journal 37(5), 1000–1024.

Freeze, R. A. and J. A. Cherry (1979). Groundwater. Upper Saddle River, NJ 07458: Prentice Hall, Inc.

Hirabayashi, Y., R. Mahendran, S. Koirala, L. Konoshima, D. Yamazaki, S. Watanabe, H. Kim, and S. Kanae (2013). Global flood risk under climate change. Nature Climate Change 3, 816–821.

Horikoshi, K. and A. Takahashi (2015). Suffusion-induced change in spatial distribution of fine fractions in embankment subjected to seepage flow. Soils and Foundations 55(5), 1293–1304.

Hunter, R. and E. Bowman (2018). Visualisation of seepage-induced suffusion and suffosion within internally erodible granular media. Géotechnique 1(1), 1–13.

Indraratna, B., J. Israr, and M. Li (2018). Inception of geohydrulic failures in granular soils – an experimental and theoretical treatment. Géotechnique 68(3), 233–248.

Indraratna, B., A. K. Raut, and H. Khabbaz (2007). Constriction-based retention criterion for granular filter design. Journal of Geotechnical and Geoenvironmental Engineering 133(3), 266–276.

Jiang, M., J. Konrad, and S. Leroueil (2003). An efficient technique for generating homogeneous specimens for dem studies. Computers and Geotechnics 30(7), 579–597.

Ke, L. and A. Takahashi (2014a). Experimental investigations on suffusion characteristics and its mechanical consequences on saturated cohesionless soil. Soils and Foundations 54(4), 713–730.

Ke, L. and A. Takahashi (2014b). Triaxial erosion test for evaluation of mechanical

consequences of internal erosion. Geotechnical Testing Journal 37(2), 347–364.

Ke, L. and A. Takahashi (2016). Drained monotonic responses of suffusional cohesionless soils. Journal of Geotechnical and Geoenvironmental Engineering 141(8), 04015033.

Kenney, T. and D. Lau (1985). Internal stabilitiy of granular filters. Canada Geotechnical Journal 22(2), 215–225.

Ladd, R. (1978). Preparing test specimens using undercompaction. Geotechnical Testing Journal 1(1), 16–23.

Liu, Y., L. Wang, Y. Hong, J. Zhao, and Z.-Y. Yin (2020). A coupled CFD-DEM investigation of suffusion of gap graded soil: Coupling effect of confining pressure and fines content. International Journal for Numerical and AnalyticalMethods in Geomechanics 44(18), 2473–2500.

Lade, P., C. Liggio, and J. Yamamuro (1998). Effects of non-plastic fines on minimum and maximum void ratios of sand. Geotechnical Testing Journal 21(4), 336–347.

Nguyen, C. D., N. Benahmed, E. And`o, L. Sibille, and P. Philippe (2019). Soil microstructural changes induced by suffusion: x-ray computed tomography characterization. E3S Web Conference 92, 01010.

Ouyang, M. (2016). Experimental investigation nd microscopic observation on internal erosion of cohesionless soils. Ph. D. thesis, Tokyo Institute of Technology.

Ouyang, M., Y. Ito, and T. Tokunaga (2020). Local land subsidence exacerbates inundation hazard to the Kujukuri Plain, Japan. Proceedings of the International Association of Hydrological Sciences 382, 657–661.

Ouyang, M., Y. Ito, and T. Tokunaga (2021a). Effects of geomorphological and geohydrological features on flood hazard in a coastal basin. Natural Hazards.

Ouyang, M., Y. Ito, and T. Tokunaga (2021b). Quantifying the inundation impacts of earthquake-induced surface elevation change by hydrological and hydraulic modeling. Scientific Reports 11(1), 4269.

Ouyang, M. and A. Takahashi (2015). Optical quantification of suffusion in plane strain physical models. Géotechnique Letters 5(3), 118–122.

Ouyang, M. and A. Takahashi (2016a). Influence of initial fines content on fabric of soils subjected to internal erosion. Canada Geotechnicla Journal 53(2), 299–313.

Ouyang, M. and A. Takahashi (2016b). Reply to the discussion by ahmad alsakran et al. on ”influence of initial fines content on fabric of soils subjected to internal erosion“. Canada Geotechnical Journal 53(8), 1358–1359.

Prasomsri, J. and A. Takahashi (2020). The role of fines on internal instability and its impact on undrained mechanical response of gap-graded soils. Soils and Foundations 60(6), 1468–1488.

Richards, K. and K. Reddy (2010). True triaxial piping test apparatus for evaluation of piping potential in earth structures. Geotechnical Testing Journal 33(1), 83–95.

Richards, K. and K. Reddy (2012). Experimental investigation of initiation of backward erosion piping in soils. Géotechnique 62(10), 933–942.

Rosenbrand, E. and J. Dijkstra (2012). Application of image subtraction data to quantify suffusion. Géotechnique Letters 2(2), 37–41.

Shire, T., C. O’Sullivan, and K. J. Hanley (2016). The influence of fines content and size-ratio on the micro-scale properties of dense bimodal materials. Granular Matter 18(3), 52.

Silveira, A. (1965). An analysis of the problem of washing through in protective filters. In Proceedings of the 6th international conference on soil mechanics and foundation

engineering, Montréal, Que, pp. 551–555.

Skempton, A. and J. Brogan (1994). Experiments on piping in sandy gravels. Géotechnique 22(4), 564–578.

Sladen, J., R. D'Holander, and J. Krahn (1985). The liquefaction of sands, a collapse surface approach. Canada Geotechnical Journal 22(4), 564–578.

Slangen, P. and R. J. Fannin (2017). The role of particle type on suffusion and suffosion. Géotechnique Letters 7(1), 6–10.

Takahashi, A. (2016). Closure to "drained monotonic responses of suffusional cohesionless soils" by lin ke and akihiro takahashi. Journal of Geotechnical and Geoenvironmental Engineering 142(5), 07016006.

Tomlinson, S. and Y. Vaid (2000). Seepage forces and confining pressure effects on piping erosion. Canada Geotechnical Journal 37(1), 1–13.

van Baaren, J. P. (1979). Quick-look permeability estimates using sidewall samples and porosity logs. In Transactions on 6th Annal European Logging Symposium, Society of Professional Well Log Analysts.

Wanatowski, D. and J. Chu (2006). Stress-strain behavior of a granular fill measured by a new plane-strain apparatus. Geotechnical Testing Journal 29(2), 1–9.

Xiao, M. and N. Shwiyhat (2012). Experimental investigation of the effects of suffusion on physical and geomechanical characteristics of sandy soils. Geotechnical Testing Journal 35(6), 890–900.

Xie, L., X. Liang, and T. Su (2018). Measurement of pressure in viewable hole erosion test. Canada Geotechnical Journal 55(10), 1502–1509.

Yang, J. and X. Liu (2016). Shear wave velocity and stiffness of sand: the role of non-plastic

fines. Géotechnique 66(6), 500–514.

Yang, J., Z.-Y. Yin, F. Laouafa, and P.-Y. Hicher (2019a). Analysis of suffusion in cohesionless soils with randomly distributed porosity and fines content. Computers and Geotechnics 111, 157–171.

Yang, J., Z.-Y. Yin, F. Laouafa, and P.-Y. Hicher (2019b). Internal erosion in dike-on-foundation modeled by a coupled hydromechanical approach. International Journal for Numerical and Analytical Methods in Geomechanics 43(3), 663–683.

Yang, J., Z.-Y. Yin, F. Laouafa, and P.-Y. Hicher (2019c). Modeling coupled erosion and filtration of fine particles in granular media. Acta Geotechnica 14(6), 1615–1627.

Yang, J., Z.-Y. Yin, F. Laouafa, and P.-Y. Hicher (2020). Hydromechanical modeling of granular soils considering internal erosion. Canadian Geotechnical Journal 57(2), 157–172.

Zhong, C., V. Le, F. Bendahmane, D. Marot, and Z. Yin (2018). Investigation of spatial scale effects on suffusion susceptibility. Journal of Geotechnical and Geoenvironmental Engineering 144(9), 04018067.

Zlatovic, S. and K. Ishihara (1997). Normalized behavior of very loose non-plastic soils: effects of fabric. Soils and Foundations 37(4), 47–56.

Zou, Y., C. Chen, and L. Zhang (2020). Simulating progression of internal erosion in gap-graded sandy gravels using coupled CFD-DEM. International Journal of Geomechanics 20(1), 04019135.

Zuo, L. and B. A. Baudet (2015). Determination of the transitional fines content of sand-non plastic fines mixtures. Soils and Foundations 55(1), 213–219.

Table 1. Properties of tested materials

Parameter	Silica no. 3	25% mixtures	Blue silica no. 8
Maximum void ratio	0.94	0.77	1.33
Minimum void ratio	0.65	0.37	0.70
Median particle size [mm]	1.76	1.69	0.16
Curvature coefficient	0.96	8.54	0.99
Uniformity coefficient	1.31	16.4	1.05

Table 2. Test conditions

Case	Consolidation	Seepage test	Drained compression test
PS_CON	Yes	No	No
PS_WOE	Yes	No	Yes
PS_WE_N1	Yes	Yes	Yes
PS_WE_N2	Yes	Yes	Yes

Table3. Seepage test results

Case	[1] [%]	[2]	[3] [%]	[4]	[5] [%]	[6]	[7] [%]	ε_v [8] [%]
PS_WE_N1	25	0.6	42	0.6	21.2	0.65	31	2
PS_WE_N2	25	0.6	42	0.6	21.2	0.65	31	2

[1] Initial fines content, [2] Initial void ratio, [3] Initial relative density, [4] Void ratio after consolidation,
[5] Fines content after seepage test, [6] Void ratio after seepage test,
[7] Relative density after seepage test, [8] Volumetric strain during seepage test.

Table 4. Drained compression test results

Case	[1] [%]	[2]	q^3 [kPa]
PS_WOE	25.0	0.60	265.9
PS_WE_N1	21.3	0.65	202.8
PS_WE_N2	21.3	0.65	204.9

[1] Fines content before drained compression test, [2] Void ratio before drained compression test,
[3] Soil peak strength.

FIGURE 1: Schematic diagram of the developed plane strain erosion apparatus.

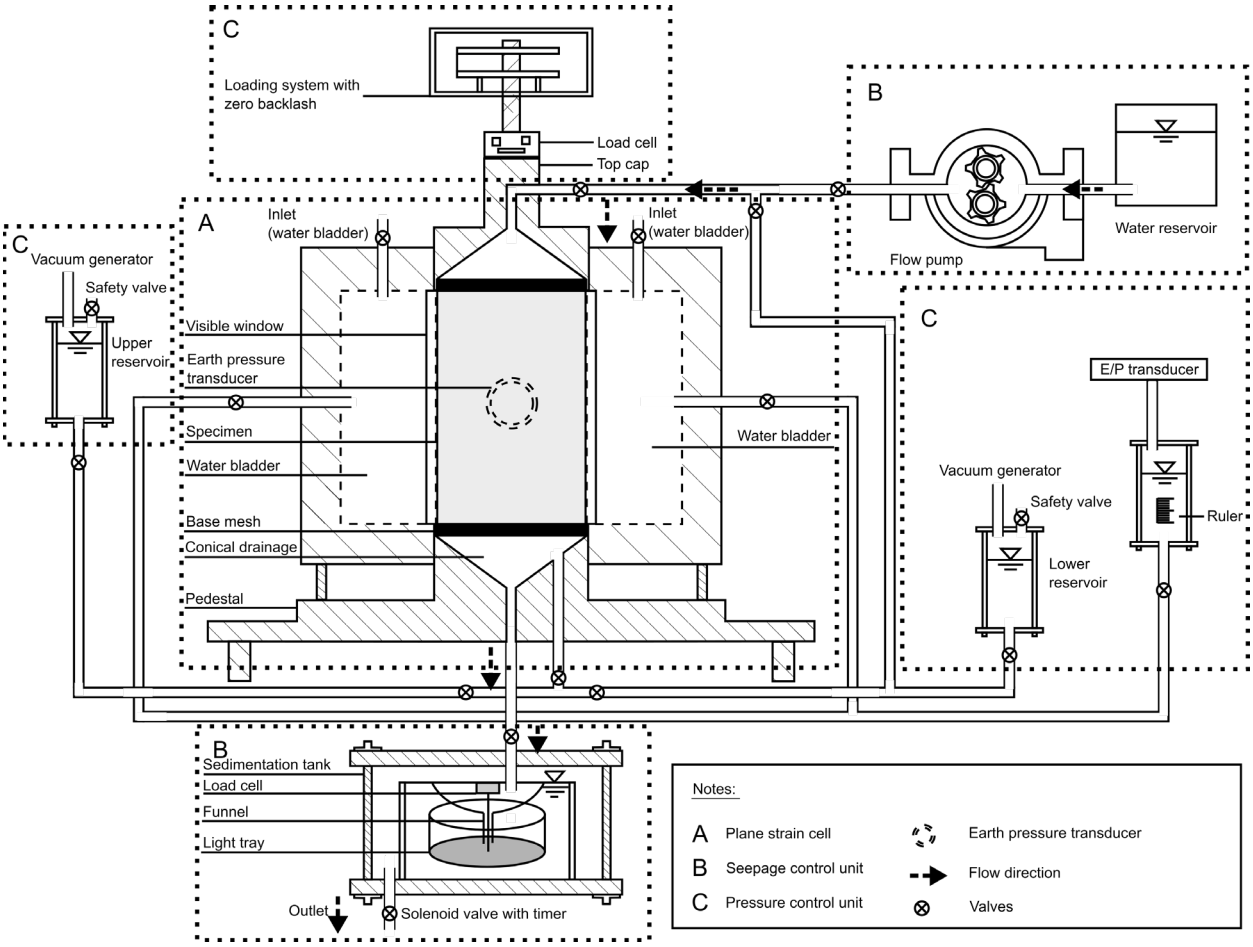

FIGURE 2: Photography of the main part of plane strain erosion apparatus.

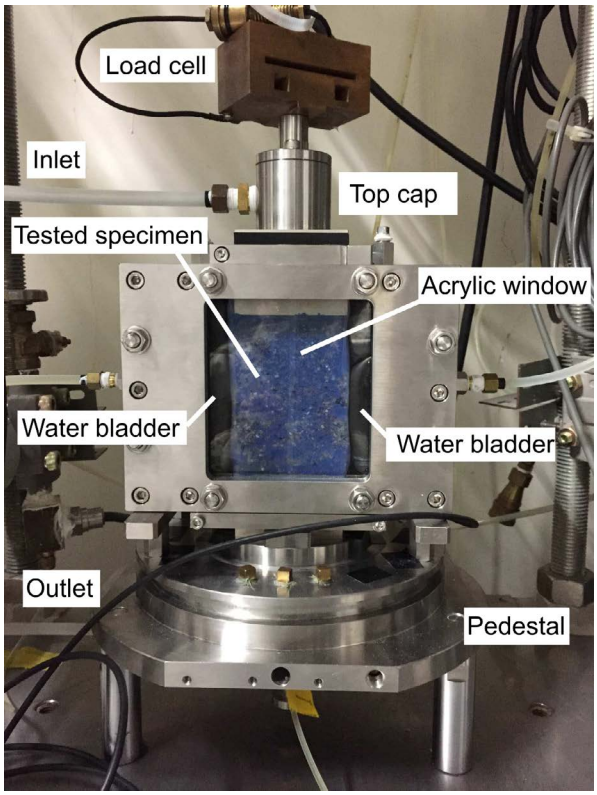

FIGURE 3: Photography of the apparatus parts; (a) top cap; (b) bottom pedestal.

(a) The top cap

(b) The bottom pedestal

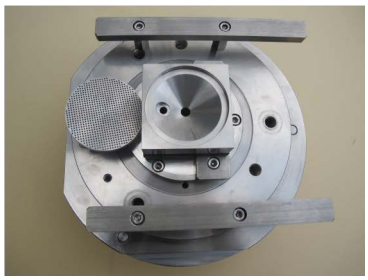

FIGURE 4: Particle size distribution curves and microscopic image of tested materials.

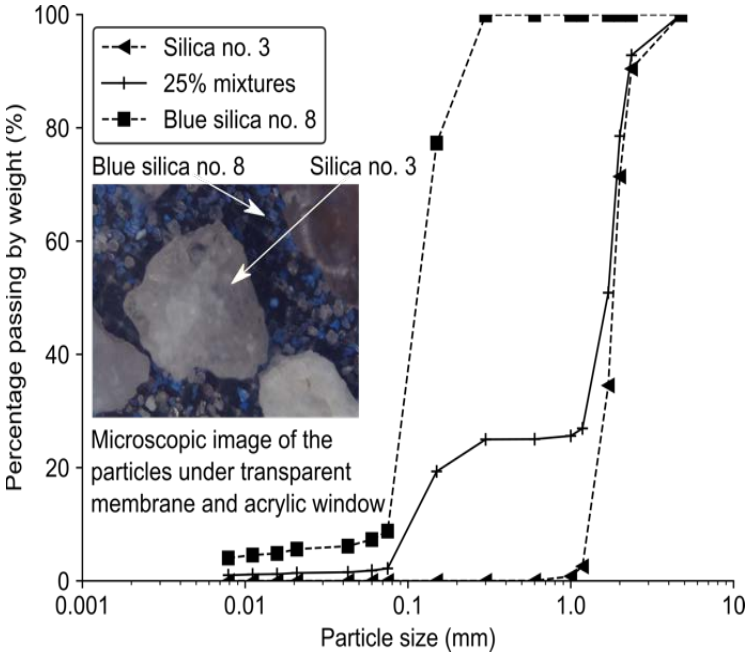

FIGURE 5: Stress conditions during the experiment.

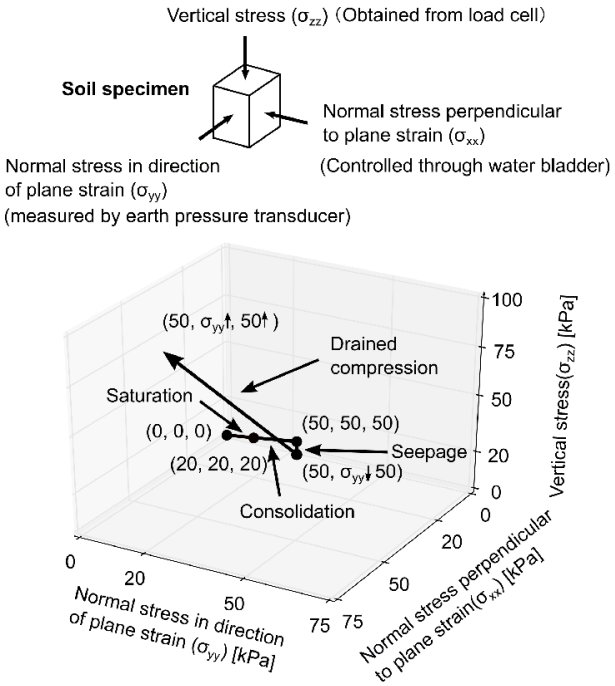

FIGURE 6: Applied flow rate in the seepage test.

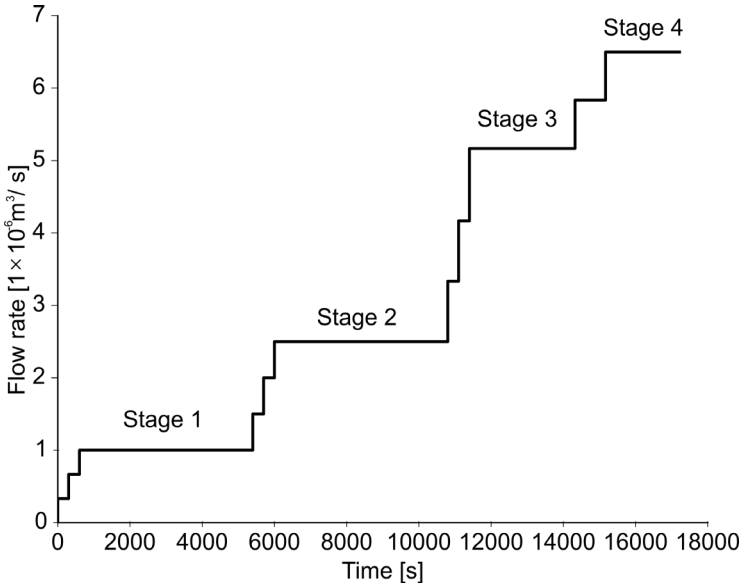

FIGURE 7: The optical results during the experiment.

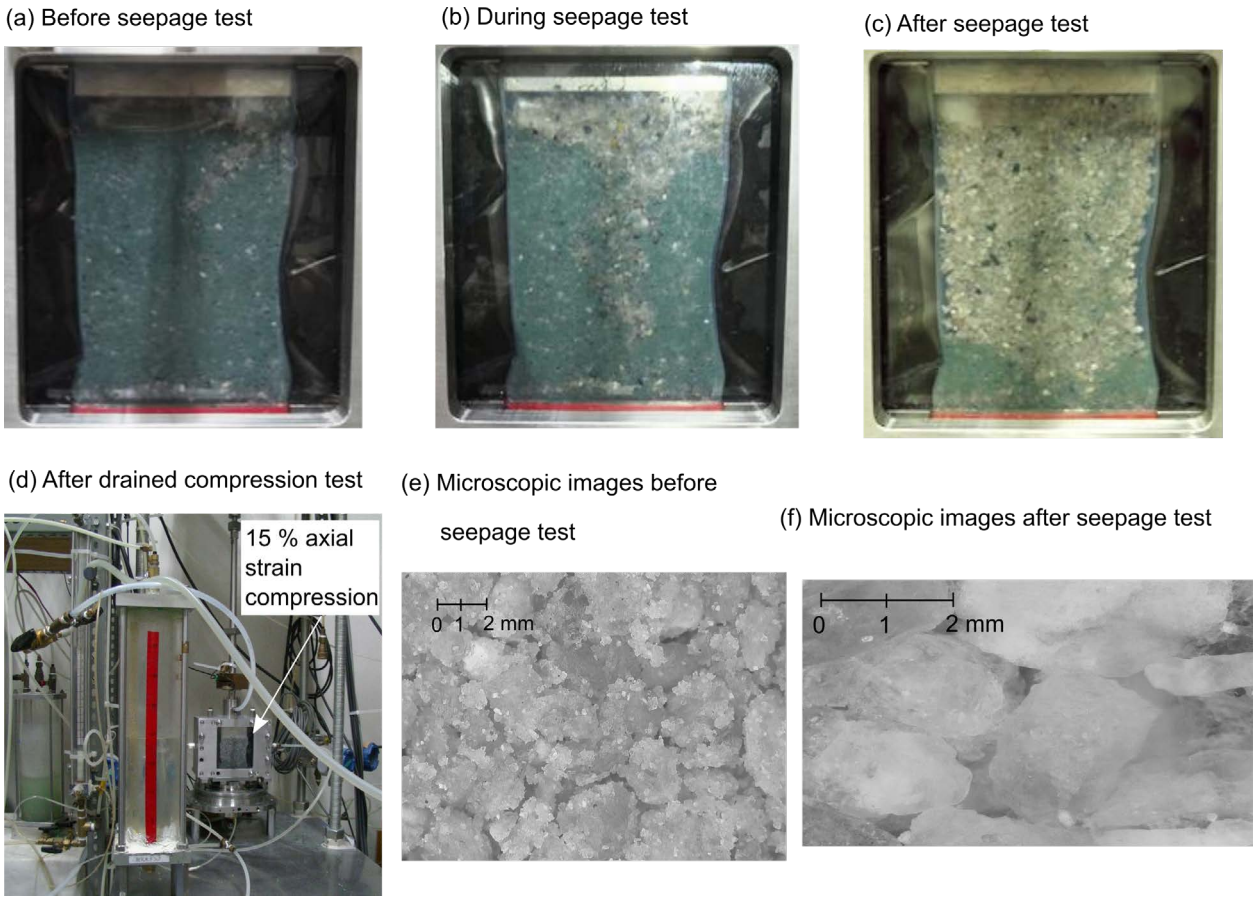

FIGURE 8: The particle size distributions of the eroded specimen.

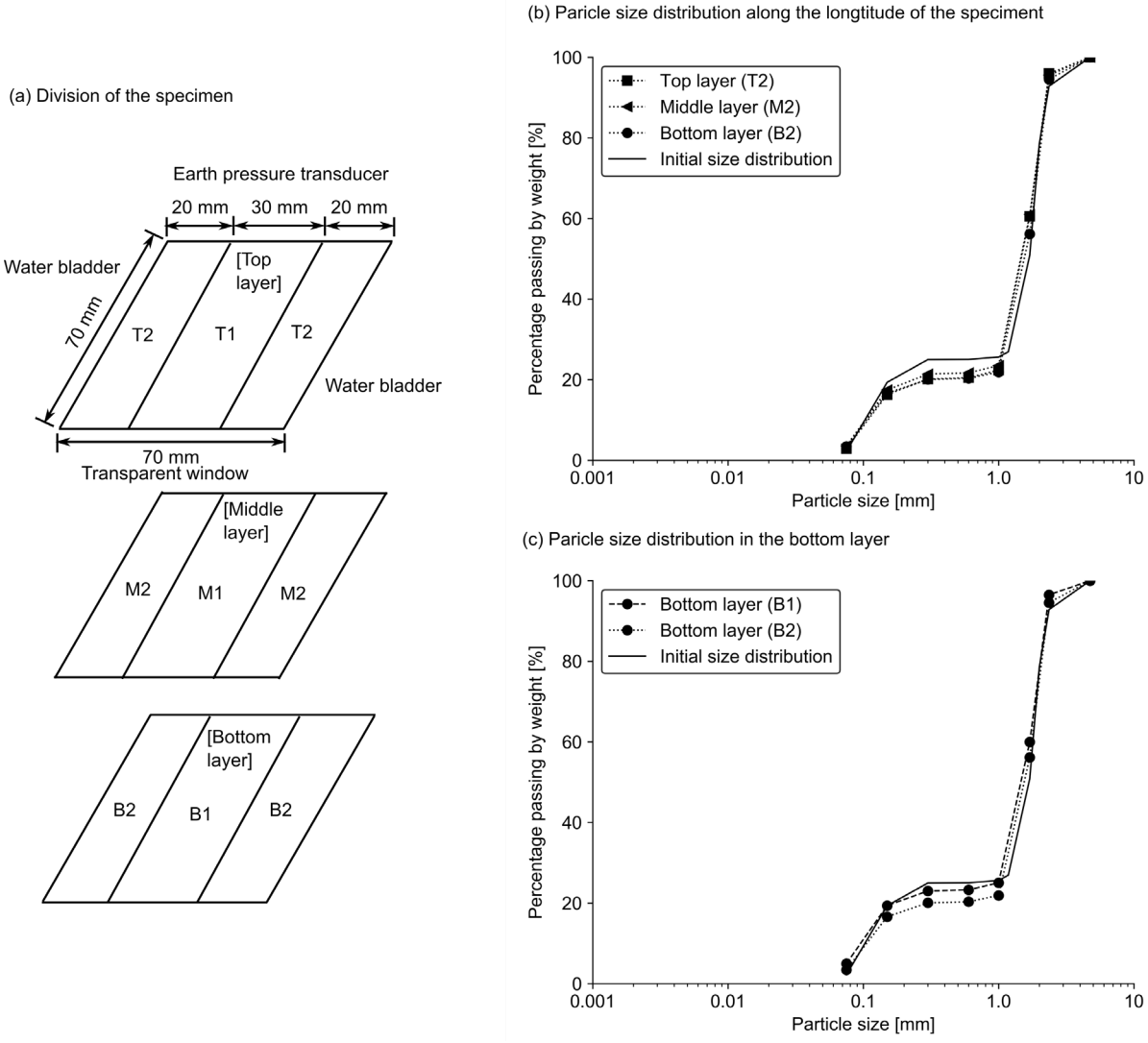

FIGURE 9: Evolutions of cumulative eroded soil mass and horizontal normal stress in direction of plane strain at the beginning of seepage test (case PS_WE_N1).

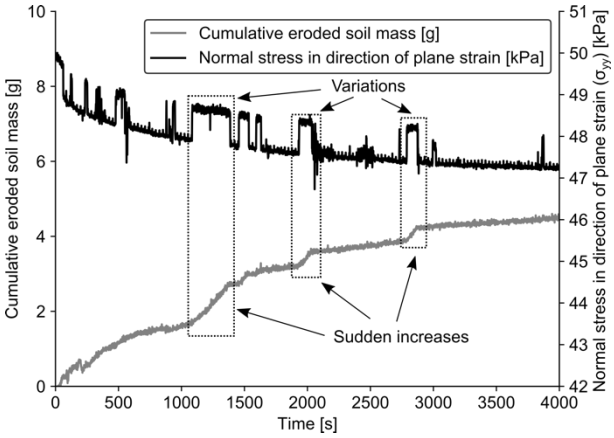

FIGURE 10: Seepage test results. (a) Evolutions of cumulative eroded soil mass; (b) Evolutions of horizontal normal stress in the direction of plane strain ($_{yy}$); (c) Evolutions of the permeability during the seepage test.

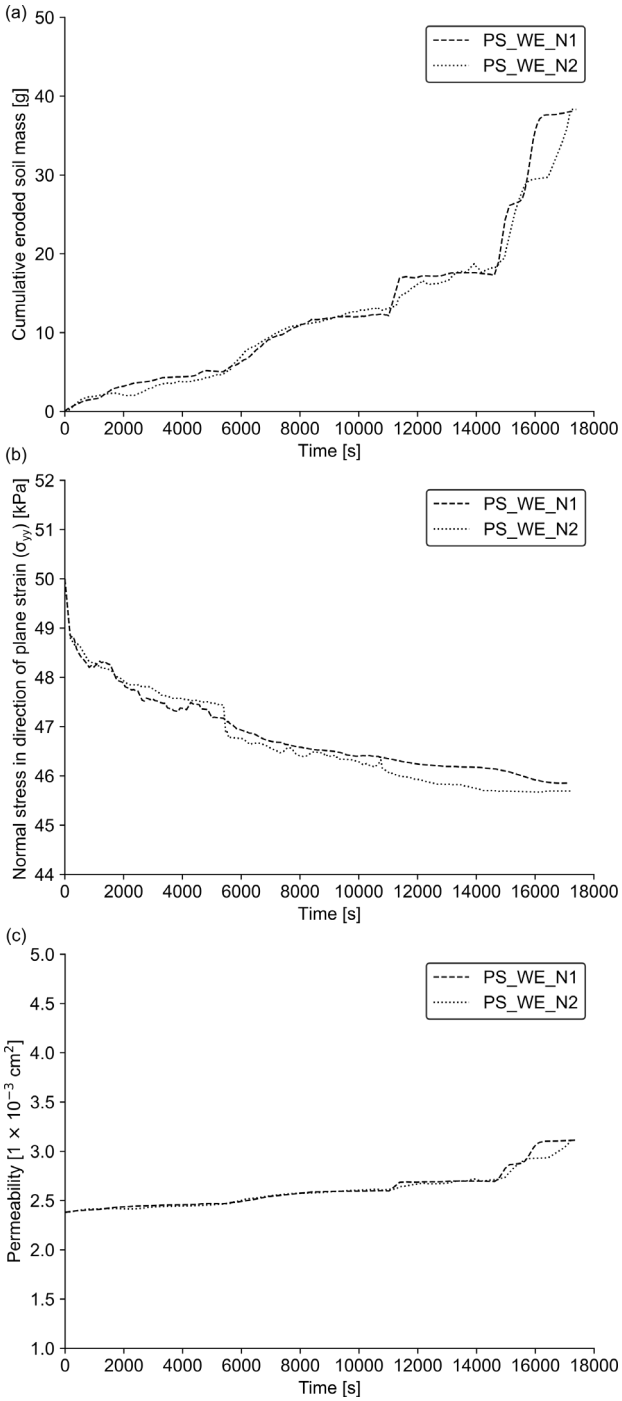

FIGURE 11: Drained compression test results. (a) Relationship of axial strain and volumetric strain; (b) Relation between axial strain and deviator stress during the whole drained compression tests; (c) Detailed stress-strain relationship at small strain level; (d) Normalized secant stiffness at small strain level.

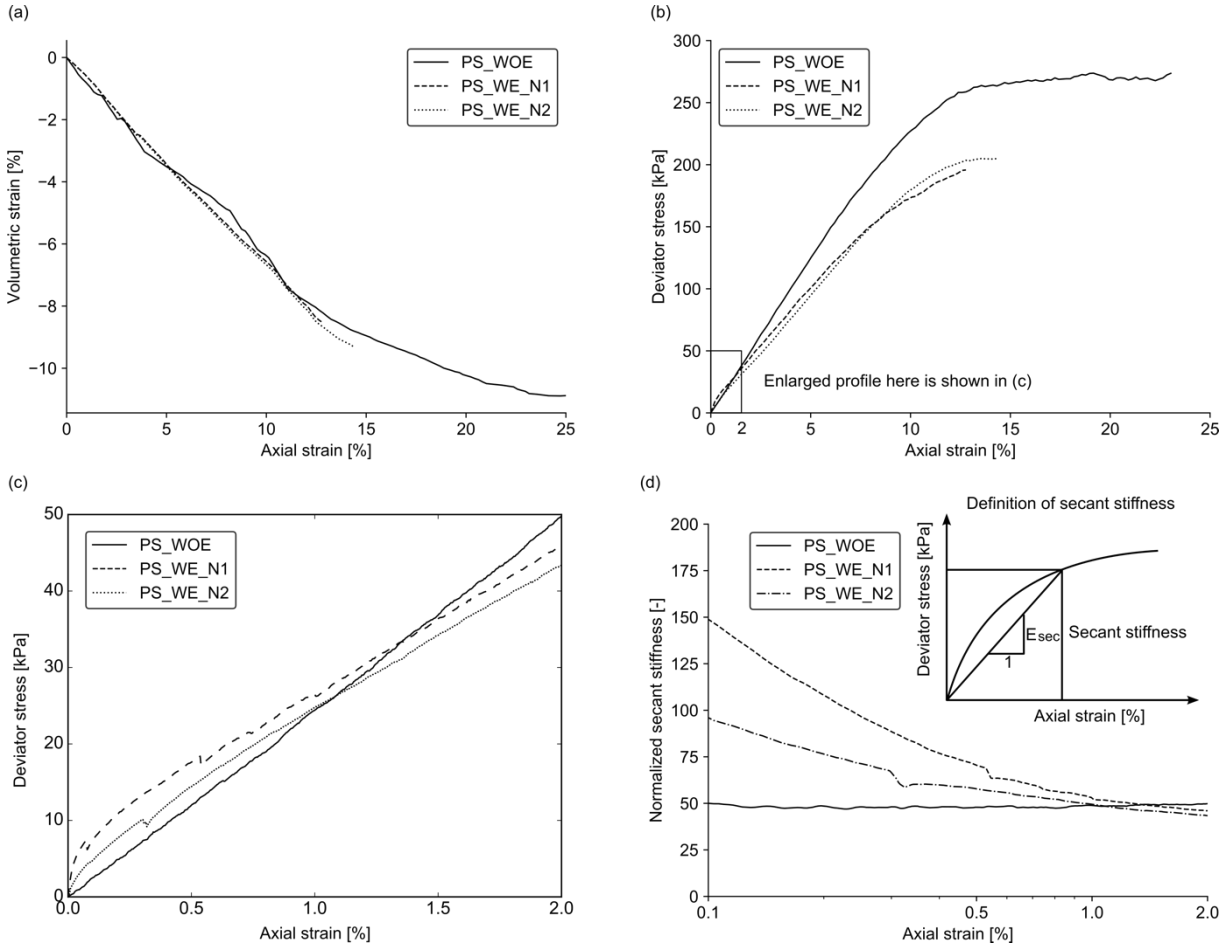

FIGURE 12: Discussions on the difference of mechanical behavior of soils with and without internal erosion. (a) Key states in the test procedure; (b) The original image and the corresponding developed schematic diagram; (c) Microstructure of soils without erosion at key states; (d) Microstructure of soils with erosion at key states. The back solid lines between particles in (c) and (d) represent the contacts between coarse particles; and white solid lines mean the contacts with fines.

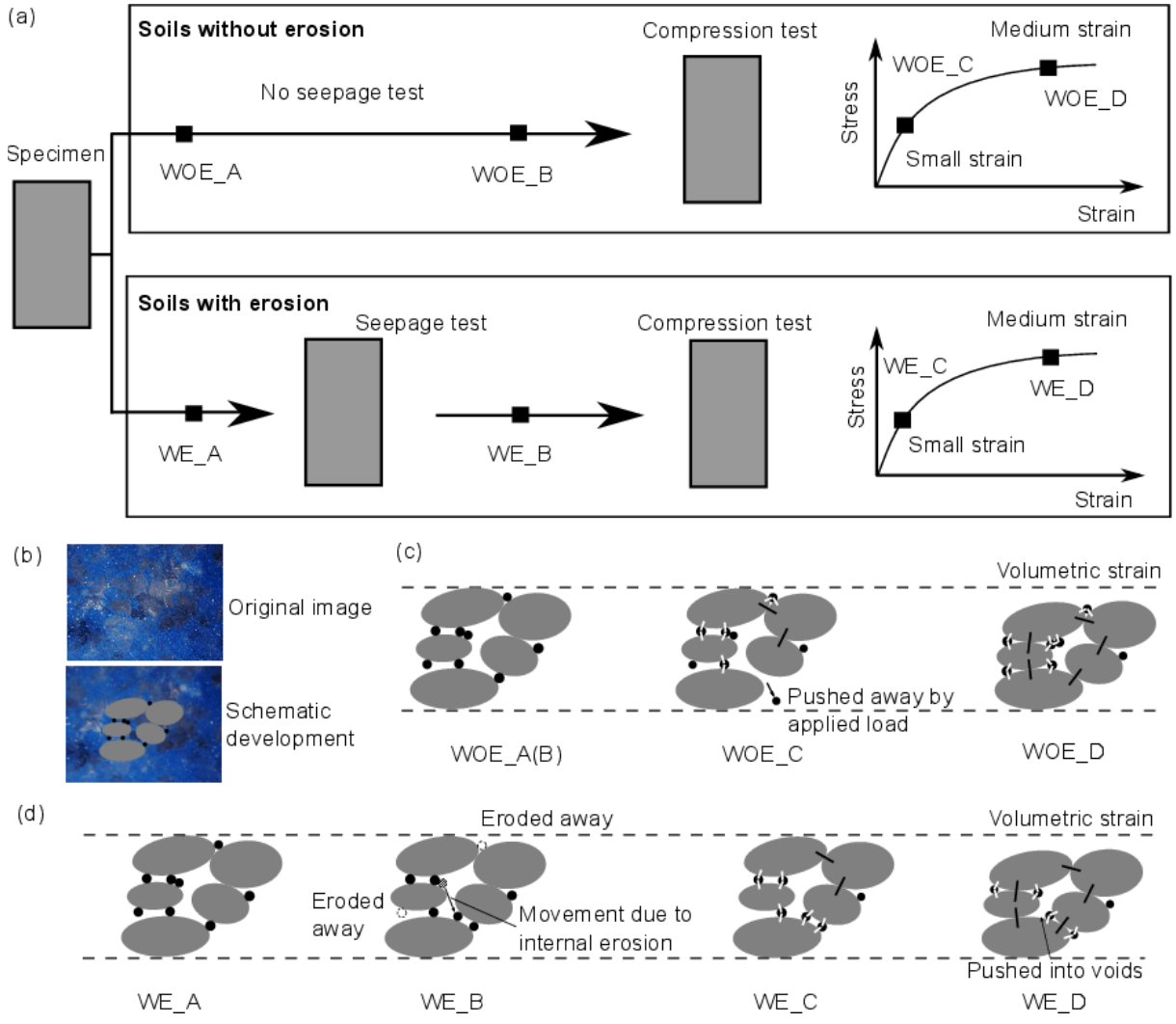

FIGURE 13: Demonstration of the area surrounded by coarse particles where fines possibly transfer the load at both densest and loosest states, .

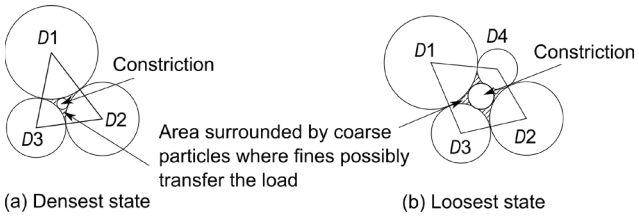

FIGURE 14: Influential factors for the calculation of the area surrounded by coarse particles where fines possibly transfer the load, .

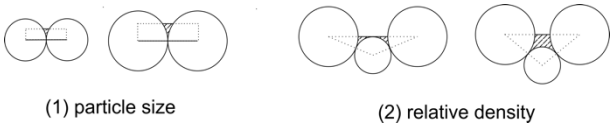

FIGURE 15: The distribution curves of .

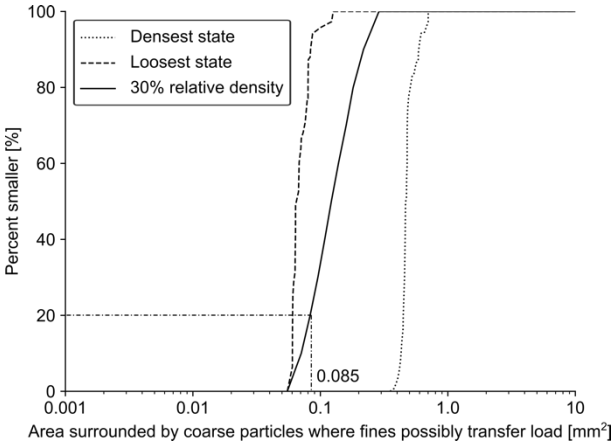

FIGURE 16: Change in fines percentage in of soils with and without internal erosion at both small and medium strain levels.